


Article

FY-3E Satellite Plasma Analyzer

Zheng Tian ^{1,2,*}, Aibing Zhang ^{1,2}, Xiangzhi Zheng ^{1,2}, Linggao Kong ^{1,2}, Bin Su ^{1,2} , Bin Liu ^{1,2}, Jianjing Ding ^{1,2}, Wenjing Wang ^{1,2}, Chao Liu ^{1,2}, Yulong Lv ^{1,2}, Jun Gao ^{1,2} and Ling Ma ³

¹ National Space Science Center, Chinese Academy of Sciences, Beijing 100190, China; zhab@nssc.ac.cn (A.Z.); zxz@nssc.ac.cn (X.Z.); klg@nssc.ac.cn (L.K.); subin@nssc.ac.cn (B.S.); liubin@nssc.ac.cn (B.L.); dj@nssc.ac.cn (J.D.); wangwenjing@nssc.ac.cn (W.W.); liuch@nssc.ac.cn (C.L.); lvyulong@nssc.ac.cn (Y.L.); gaojun@nssc.ac.cn (J.G.)

² Beijing Key Laboratory of Space Environment Exploration, Beijing 100190, China

³ School of Integrated Circuits and Electronics, Beijing Institute of Technology, Beijing 100081, China; 50026@bit.edu.cn

* Correspondence: tianzheng@nssc.ac.cn

Abstract: The FY-3E satellite plasma analyzer marks China's first detection of the characteristics, occurrence, and development of the typical plasma environment in the dawn–dusk orbit space. It provides data source support for operational space weather alerts and forecasts, helps ensure the in-orbit safety of the satellite, and accumulates space environment detection data for space environment modeling and space physics research. This paper gives a detailed introduction to the detection technology adopted by the FY-3E satellite plasma analyzer. We calibrated its performance through a calibration experiment and then analyzed and compared it with similar instruments in China. It is indicated that the instrument is capable of measuring an ion energy spectrum of 24 eV~32 keV and an electron energy spectrum of 23.7 eV~31.6 keV, its field of view reaches $180^\circ \times 90^\circ$, and the inversed measurement range of spacecraft absolute potential is better than $-30\text{ kV} \sim +30\text{ kV}$. All these contribute to a notably improved technology for plasma and satellite potential detection of China's LEO satellites.

Keywords: low Earth orbit (LEO); absolute potential; electrostatic analyzer; energy spectrum; electrostatic discharge (ESD); field of view; UV suppression



Citation: Tian, Z.; Zhang, A.; Zheng, X.; Kong, L.; Su, B.; Liu, B.; Ding, J.; Wang, W.; Liu, C.; Lv, Y.; et al. FY-3E Satellite Plasma Analyzer. *Atmosphere* **2024**, *15*, 14. <https://doi.org/10.3390/atmos15010014>

Academic Editor: Victor Ivanovich Zakharov

Received: 8 November 2023

Revised: 6 December 2023

Accepted: 9 December 2023

Published: 21 December 2023



Copyright: © 2023 by the authors. Licensee MDPI, Basel, Switzerland. This article is an open access article distributed under the terms and conditions of the Creative Commons Attribution (CC BY) license (<https://creativecommons.org/licenses/by/4.0/>).

1. Introduction

A low-Earth orbit meteorological satellite is mainly responsible for providing global observation data meeting time and space requirements for numerical weather prediction in order to improve the timeliness and accuracy of the prediction. The WMO Vision for Global Observing Systems in 2025 proposes to equip polar-orbiting satellite platforms with particle detection instruments for space weather monitoring [1]. It is shown in Table 1 below.

Table 1. Polar-orbiting sun-synchronous satellites that have been or will be operated between 2014 and 2025.

Title 1	2014	2025
Early morning (LECT~1730)	DMSP F-16, -17, -19	DMSP F20 FY-3E, 3G
Morning (LECT~0930)	Metop-A, -B DMSP-18 FY-3C Meteor-M N1, -N2	Metop-C Metop-SG Meteor-M N2
Afternoon (LECT~1330)	NOAA-15, -18, -19 Suomi-NPP FY-3B	JPSS-1, -2 FY-3F
(LECT~1530)		Meteor-M N2, -MP

FY-3E is the first dawn–dusk orbit meteorological satellite of the “Fengyun” satellite family and also the world’s first sun-synchronous meteorological satellite routinely operating in a dawn–dusk orbit [2]. It forms a dawn–morning–afternoon network with the in-orbit FY-3C and FY-3D satellites to achieve 100% coverage of global observation data [3].

FY-3E satellite was launched on 5 July 2021, bringing the “plasma analyzer” developed by the space probe technical team to the dawn to dusk low Earth orbit for the first time, in response to WMO’s requirement for polar-orbiting particle observations. The plasma analyzer is mainly responsible for monitoring the characteristics, occurrence, and development of the typical plasma environment in the dawn–dusk orbit space, providing data sources for operational space weather alerts and forecasts, and accumulating space environment detection data for space environment modeling and space physics research. Compared with instruments of the same type, such as the SSI/ES payload of the DMSP [4] satellite, the ESAs payload of the THEMIS satellite [5], the SEM-2 of the latest NOAA18, and 19 of the POES series satellites [6], FY-3E satellite plasma analyzer has reached and partially exceeded the level of similar instruments in terms of performance indexes.

2. Scientific and Application Objectives of the Instrument

Particle precipitation is a space weather effect where high-energy particles are injected into the upper atmosphere of the Earth, causing disturbances in the ionosphere and thermosphere, and even ionospheric holes or enhancements, thereby having a significant impact on ground-based and space technology systems. Precipitating particles are mainly from radiation belts, ring currents, solar wind, and solar cosmic rays. During a solar storm, plasma ions and electrons from the above regions are accelerated toward the Earth, and injected into the ionosphere and thermosphere from the poles and middle and high latitudes.

The observation and research of precipitating particles are of great significance for explaining the process of solar wind–magnetosphere–ionosphere coupling. Energetic particles injected into the ionosphere trigger a pitch angle scattering through collisions and wave–particle interactions, which causes hot plasmas from the ring current, the solar wind, and the plasma sheet to enter the Earth’s upper atmosphere and ionosphere, so that the energy-charged particles collide with neutral atmosphere+ to undergo energy losses and generate precipitating particles. The injected particles interact with the constituent particles of the Earth’s upper atmosphere and cause light emissions that are seen as aurora in the polar ionospheres. The precipitating particles also cause enhanced ionospheric ionization, compositional changes of the constituent particles of the atmosphere, enhanced ionospheric conductivity, and temperature changes in the atmosphere. Different processes in the interplanetary space and the magnetosphere may lead to the precipitation of high-energy charged particles into the ionosphere. During a magnetic storm, the high-speed blasts of solar wind and the southward interplanetary magnetic field propel high-energy charged particles deep into the inner magnetosphere. Generally, electron precipitation carries most of the particle energy and is the primary driver of high-latitude ionospheric auroras. However, for certain locations and times, such as the equatorial edge of the auroral oval, proton precipitation can be the major energy source of ionization and excitation and, thus, the primary contributor to auroral emissions.

As a sun-synchronous orbit satellite at an altitude of 836 km, FY-3E orbits the Earth from pole to pole, making it the optimal location for monitoring the injection of precipitating particles during solar storms. Since electrons and protons below 40 keV play an important role in energy transfer within the Earth’s magnetosphere and into the high-latitude ionosphere, the plasma analyzer is equipped with the capability of monitoring electrons and protons of 10 eV–30 keV in the Earth’s magnetosphere. The research on precipitating particles was at first derived from the research on auroral particle precipitation. The absolute potential detection of spacecraft by plasma detection equipment has a long history [7]. Therefore, the scientific objective of the plasma analyzer is to carry out comprehensive detection of the thermal plasma environment and surface charge–discharge effects in the orbit of the polar-orbiting satellite, and to capture the flux and energy spectral distribution of

precipitating particles, catering to the research on ionospheric and thermospheric response and change caused by particle precipitation.

FY-3E satellite has an observation altitude of about 830 km in the ionosphere. The installed plasma analyzer mainly focuses on precipitating particles produced by hot plasma electrons and ions of the ring current of about 1 keV–300 keV, the solar wind with an average energy of 1 keV, and the magnetospheric plasma sheet of 10 eV–10 keV. However, the precipitating particles that produce more notable aurora are mainly distributed in the low energy spectrum, leading to visible aurora particles of 0.5 keV~20 keV and >20 keV, while the high energy spectrum has no significant effect on the auroral emission. Combined with the observation results of Polar and DMSP, the payload is designed to be in the energy range 300 eV~30 keV, with an energy resolution of 0.12 ($\Delta E/E_0$).

The +X direction of the FY-3E satellite is the direction of the flight path, and the +Z direction is the nadir direction. The plasma analyzer of the space probe is installed on the -Z side (zenith) of the satellite and the green sector is the $180^\circ \times \pm 45^\circ$ field of view of the electron sensor of the plasma analyzer, and the purple sector is the $180^\circ \times \pm 45^\circ$ field of view of the ion sensor. It is shown in Figure 1 below.

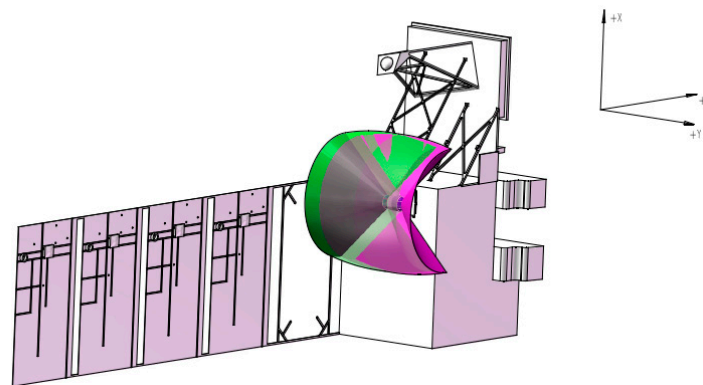


Figure 1. Installation position and detectable field of view of the FY-3E plasma analyzer.

3. Design of the FY-3E Satellite Plasma Analyzer

The Information on key design parameters of the FY-3E satellite plasma analyzer are shown in Table 2.

Table 2. Key design parameters of the FY-3E satellite plasma analyzer.

Parameters Name	Value
Outer Envelope Size	296 mm × 217 mm × 221 mm
Total Mass	4.1 kg
Power Consumption	8 Watts

3.1. Sensor Design

The “plasma analyzer” consists of an electron analyzer and an ion analyzer, both consisting of a deflection system [8,9], an electrostatic analyzer [10], and a particle collection sampling system. It works in the way shown in Figure 2 (1)~(5). In the ion sensor, for example, a negative high voltage is applied to the inner hemisphere of the electrostatic analyzer, with the outer hemisphere grounded, to form an electric field between the two hemispheres. Once entering the electrostatic analyzer through the top cover, positive ions of certain energy will be deflected under the action of the electric field between the two hemispheres. Only ions with energy matching the electric field may pass through the electrostatic analyzer and reach the outlet, while those with energy higher or lower than the electric field will hit the outer or inner hemisphere and cannot reach the outlet of the electrostatic analyzer. By varying the voltage of the inner hemisphere, we are capable of

measuring different ion energies. The relationship between ion energy, charge, and voltage is presented in this equation [11]:

$$E = kqU \quad (1)$$

where E is the ion energy, q is the ion charge, U is the voltage of the inner hemisphere, and k is the electrostatic analyzer factor (determined by the geometric parameters of the electrostatic analyzer):

$$k = \frac{(R_1 + R_2)/2}{2(R_1 - R_2)} \quad (2)$$

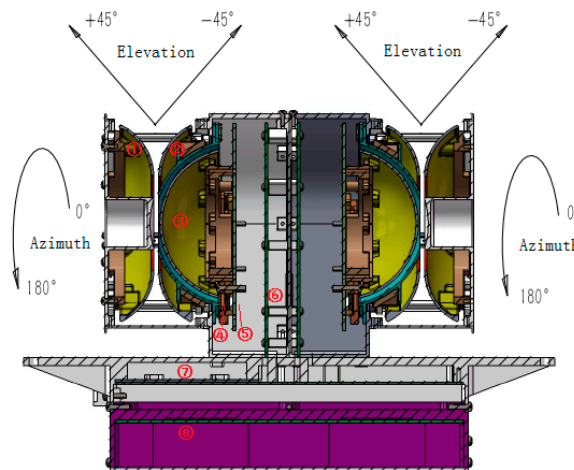


Figure 2. Cross-sectional view of the plasma analyzer. ① Deflection plate 1; ② deflection plate 2; ③ electrostatic analyzer; ④ microchannel plate; ⑤ anode system; ⑥ preamplifier system; ⑦ computer plate; ⑧ high-voltage power supply.

The inner radius R_1 of the outer spherical plate is 50 mm and the outer radius R_2 of the inner spherical plate is 47 mm. The electrostatic analyzer factor is equal to 8.08.

The electrostatic analyzer features a bending effect on the flat incident particles. Particles from different directions undergo energy filtering through the electrostatic analyzer. The microchannel plate (MCP) amplifies the outgoing particles, which are then collected through the anode plate. The microchannel plate amplifies the outgoing particles, which are then collected through the anode plate. Finally, the electronic systems perform statistical analysis on the particles' energy, quantity, and azimuthal angle.

The electron sensor and the ion sensor are arranged back-to-back, both featuring a stereoscopic $180^\circ \times 90^\circ$ field of view of about 1.4π . The electron sensor and the ion sensor each have eight anodes with an angular resolution (θ) of 22.5° . The sensor features a working cycle of 1 s, which can scan 60 energy channels and 6 elevation angles (with an elevation angle resolution of 15°), as shown in Figure 2. The figure illustrates the basic mechanical structure and electronic structure of the whole instrument and the sensor field of view.

A detailed particle trajectory simulation was carried out during the design of the plasma analyzer. The simulation is aimed at properly configuring the voltages of each electrode in the sensor to ensure that the ions go along the required flight path in the sensor. Figure 3 shows the particle trajectory simulation in the deflection system and the electrostatic analyzer. The blue lines in the figure represent the particle trajectories, and the green lines represent the electric field distribution. It can be seen from the figure that the particle deflection system can deflect the incident space ions by applying higher voltages, which meets the detection requirement of a large field of view for space particles. Particles in space can smoothly pass through the slit of the electrostatic analyzer and finally enter the electronic system at the back end for incidence azimuth analysis. The trajectory of the particles' flight is shown in Figure 3. The hemispherical electrostatic analyzer is truncated

at the bottom to facilitate the detection with MCP. The cutoff angle for the electrostatic analyzer was set to 77° .

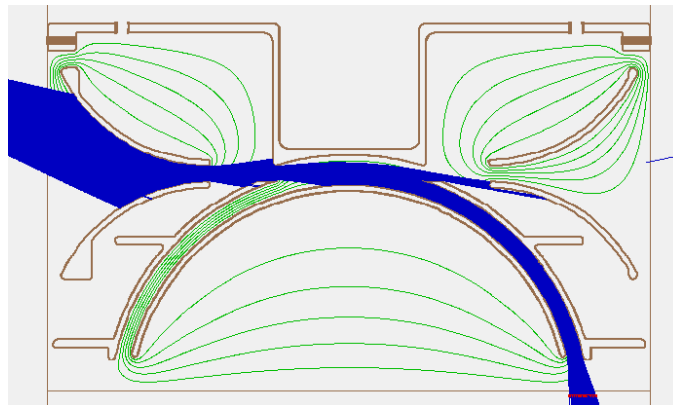


Figure 3. Particle trajectory simulation in the sensor.

Figure 4 illustrates the design of the sensor modular of the plasma analyzer, including all the parts that can be individually processed and tested. Figure 4a shows the MCP stack connected to the anode, its mounting hardware, and how it is fixed to the anode. The MCPs are equipped with spring-pressing devices on their inner and outer edges so that the dual MCPs can be tightly and evenly pressed onto the surface of the anode. The component allows individual testing of the MCPs prior to sensor assembly to verify their reliability and safety. The electron/ion sensor of the plasma analyzer is made of two 1 mm-thick microchannel plates (chevron configuration) produced by North Night Vision Technology Co., Ltd., each featuring a gain of ≥ 7000 (1000 V). The operating voltage of the dual-MCP stack was set at about 2.3 kV to amplify particle input events to $\sim 2 \times 10^6$ e and approximately -320 fC.

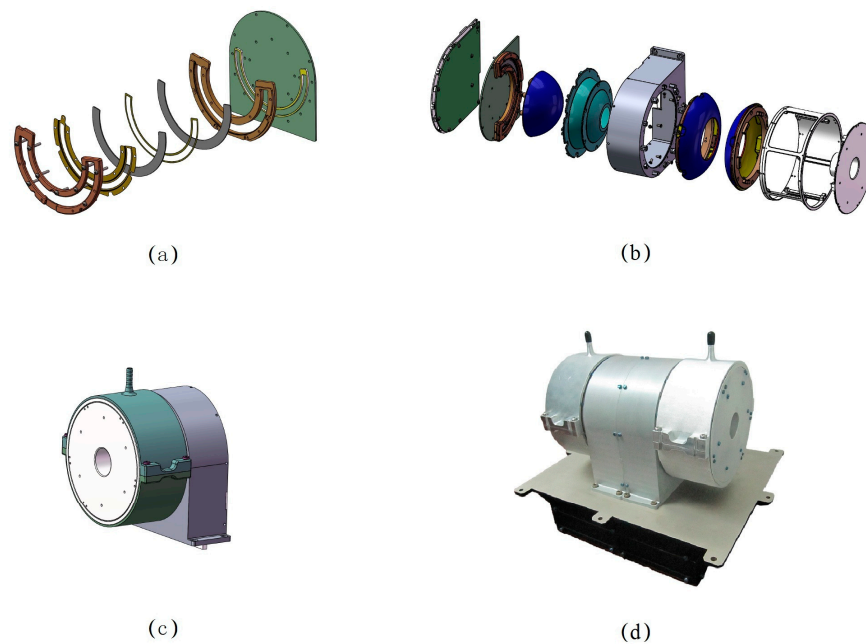


Figure 4. Sensor modular design. (a) Structures of the anode and the microchannel plate; (b) explosive view of the sensor assembly; (c) assembly of the sensor and the protective cover for nitrogen blowing; (d) the instrument assembly.

Figure 4b presents the specific structural design of the sensor. The inner hemisphere of the electrostatic analyzer is fixed at the center of the anode plate. The electrostatic analyzer has an advanced optical black finish, which is capable of absorbing stray light in ultraviolet, visible spectra, and infrared wavelengths. The black finish features extremely low reflectivity, high thermal stability, and an extremely low outgassing rate. It is used to suppress the contamination of the plasma analyzer data by sunlight. The outer hemisphere is fixed onto the sensor frame. The inner and outer hemispheres are fixed with eight equally spaced screws at 45° intervals, thus ensuring the installation accuracy of the electrostatic analyzer. To suppress the interference of ultraviolet light on the electron and ion counts of the plasma analyzer [12,13], the internationally advanced ultraviolet suppression technology is adopted to blacken the surface (vacuum coating technology called “magic black”) of the deflection plate of the particle incidence window and the electrostatic analyzer, as shown in Figure 5.



Figure 5. UV suppression: surface blackening of the deflection plate and the electrostatic analyzer.

Figure 4c shows the overall structure of the electron/ion sensor. The sensor is protected in a cover for nitrogen blowing. For the purpose of storage, the plasma analyzer is connected to the nitrogen-blowing port of the protective cover through a set of nitrogen-blowing protection systems to be fed with high-purity nitrogen (purity: 99.999%) at about 10 L/h to prevent the MCP from lattice denaturation caused by water vapor on the surface and the subsequent decrease in detection efficiency, and also to prevent dust in the sensor from contaminating the MCPs. The nitrogen-blowing protection system consists of a high-purity nitrogen cylinder, a pressure relief valve, a flow meter, a filter, etc.

3.2. Electronics Design

The electronics part of the plasma analyzer features three main functions: (a) processing the electron and ion signals output by the MCP; (b) providing high voltage for the sensor part; (c) providing power supply and communication with the external payload controller. Figure 6 is the functional block diagram of the electronics part.

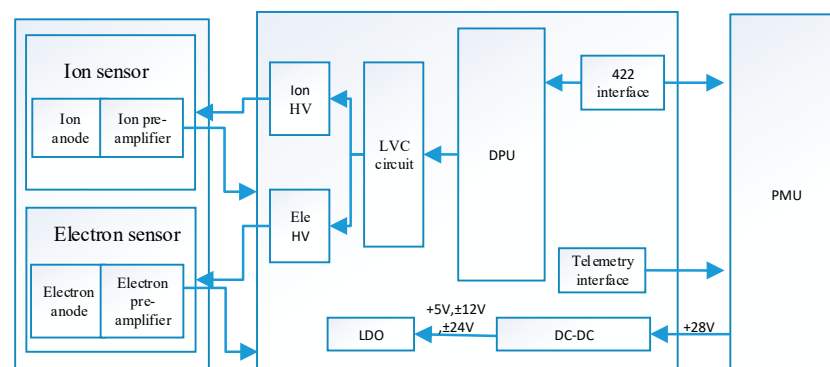


Figure 6. Block diagram of the electronics system.

The electronics box has a modular electromechanical design, with reasonably divided circuit functions enabling independent commissioning of individual circuits, thus minimizing the coupling relationship between each other and simplifying the instrument's assembly and disassembly. The electronics instrument consists of (a) an anode board, (b) a preamplifier board, (c) a power supply and computer control board, (d) a high-voltage board, (e) a low-voltage control board, and (f) a high-voltage power supply assembly.

There are eight independent anodes on the anode board. The mean radial distance of every anode (from the cylindrical axis of symmetry of the instrument) is 48 mm. A1 (Anode1) covers $0^{\circ}\sim 22.5^{\circ}$, A2 covers $22.5^{\circ}\sim 45^{\circ}$, until A8 covers $157.5^{\circ}\sim 180^{\circ}$. Each anode covers 22.5° . Considering grid transmittance and structural shielding, the fraction of charged particles that transit the top hat and are collected is about 90%. The anode is finished with gold-plated brass in a thickness of 35 μm . The anode position is determined according to the simulation results. There is ground protection between signals to avoid adjacent signal coupling. The particle signal collected by the anode is sent to the preamplifier board via an inter-board connector. The anode board is shown in Figure 7.

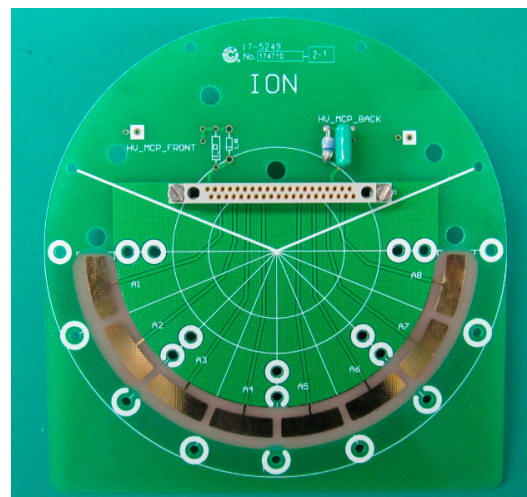


Figure 7. Independent anodes on the anode board.

The preamplifier board is provided with eight Amptek A121 charge-sensitive amplifiers corresponding to each anode. The preamplifier is used to detect the output charge pulses. The detected output pulse signal of particle events is recorded by the counter inside the FPGA on the computer control board. The FPGA allows a programmable test pulse generator for A121 amplifiers to provide test signals and cater to calibration in the absence of particle events or high voltage. The rate of the test signal can be controlled by commands sent from the ground-based system. The preamplifier threshold was set to -40 fC (about 250,000 electrons), which is high above the noise of the system.

The high-voltage circuit output sensor of the plasma analyzer requires multiple high voltages, including electron deflection high voltage 1, electron deflection high voltage 2, electron electrostatic analyzer high voltage, electron micro-channel plate high voltage, ion deflection high voltage 1, ion deflection high voltage 2, ion electrostatic analyzer high voltage, and ion micro-channel plate high voltage. The deflection high voltage is applied to the deflection plate at the entrance of the sensor, and the incident ions in different elevation angles are selected by sweeping. The electrostatic analyzer high voltage is used for the selection of the energy of the incident ions. The energy sweep is realized through a high-voltage sweep. The micro-channel plate's high voltage is used for the amplification of the micro-channel plate so that it can amplify incident particle events and output charge signals. The composition of the high-voltage system is shown in Figure 8. The electron main high-voltage circuit outputs a fixed voltage of $+3.85$ kV. The TEK HV801 high-voltage optocoupler discharges the electron deflection high-voltage circuit $1/2$, the

electron electrostatic analyzer high voltage, and the electron microchannel plate's high voltage. The ion main high-voltage circuit outputs a fixed voltage of -3.85 kV and has the same structure as the electron high-voltage circuit. The voltage range for each electrode is shown in Table 3.

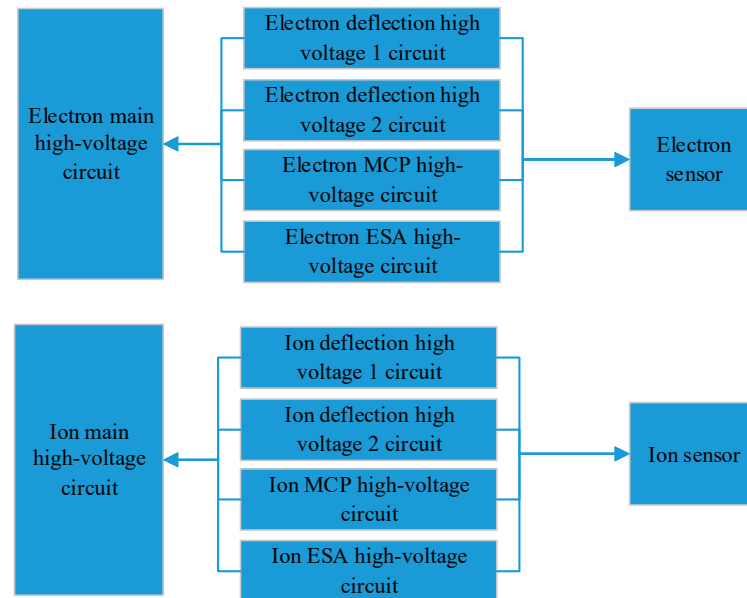


Figure 8. Functional block diagram of high-voltage power supply.

Table 3. List of high voltages for the plasma analyzer.

No.	Name	Design Output (V)	In-Orbit Range (V)	Source
1.	Electron main high voltage	0~4100	3850	Electron main high voltage
2.	Electron deflection high voltage 1	0~4100	0~3800	
3.	Electron deflection high voltage 2	0~4100	0~3800	
4.	Electron microchannel plate high voltage	0~2500	0~2200	
5.	Electron electrostatic analyzer high voltage	0~4100	0~3800	
6.	Ion main high voltage	$-4100\sim 0$	-3850	Ion main high voltage
7.	Ion deflection high voltage 1	$-4100\sim 0$	$-3800\sim 0$	
8.	Ion deflection high voltage 2	$-4100\sim 0$	$-3800\sim 0$	
9.	Electron microchannel plate high voltage	$-2500\sim 0$	$-2300\sim 0$	
10.	Ion electrostatic analyzer high voltage	$-4100\sim 0$	$-3800\sim 0$	

The electron/ion main high-voltage circuit obeys the same circuit principle, as shown in Figure 9, which consists of an oscillatory circuit, a switch circuit, a transformer, a voltage-doubling rectifier circuit, a feedback circuit, and a regulating circuit. The oscillatory circuit generates the pulse signal for the switch circuit, which is used to control the on and off of the switching circuit. Under the control of the signal generated by the oscillatory circuit, the switch circuit converts the DC signal into an AC signal, which is then supplied to the transformer. The transformer converts the low-voltage AC signals to high-voltage AC signals. The feedback circuit converts the output high voltage into a low voltage for feedback control, which is meanwhile used as the monitored value of the high voltage output. The regulating circuit enables a closed-loop control of the high voltage. The circuit board underwent a high-insulation treatment to prevent high-voltage discharge.

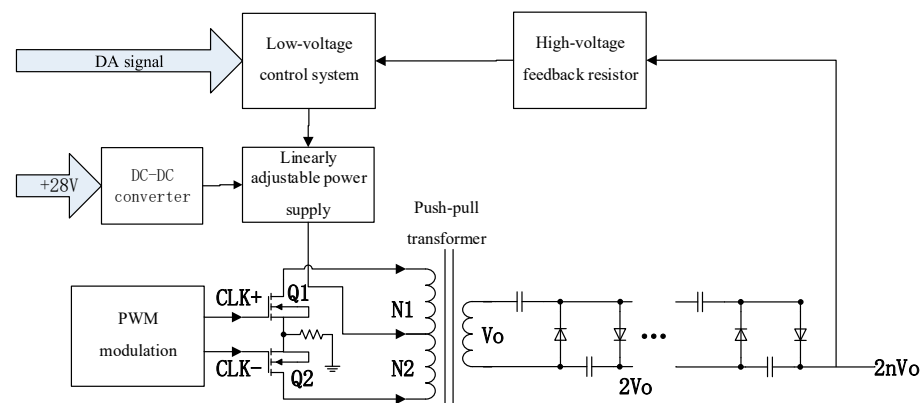


Figure 9. The working principle of main high voltage based on push-pull transformer.

The high voltage of the micro-channel plate has low requirements on the voltage change rate and accuracy, and the structure design is simple. The working principle is shown in Figure 10. The high-voltage optocoupler is for adjusting the fixed output high voltage to a variable high voltage, and the feedback circuit converts the output high voltage into a low voltage for feedback control and as the monitored value of the output high voltage. The regulating circuit enables the closed-loop control of the high voltage. The high-voltage circuit of the plasma analyzer adopts TEK HV801RH high-voltage optocoupler with an anti-irradiation index, which features a small size, an isolation voltage better than 12 kV, a low dark current, an anti-irradiation index of 100 Krads, a high voltage conversion rate, and a slew rate of up to 100 V/ μ s.

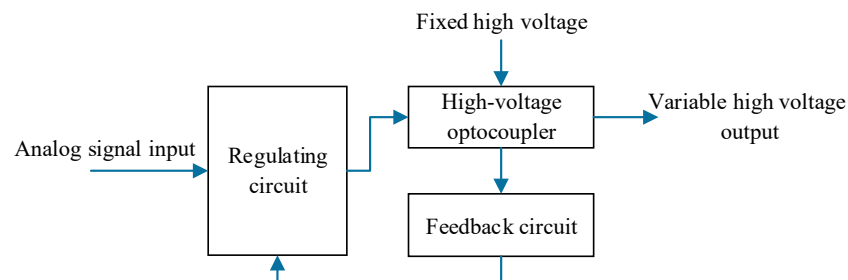


Figure 10. Variable high-voltage output circuit.

Deflection high voltage 1, deflection high voltage 2, and electrostatic analyzer high voltage need to be swept within the working cycle and require high voltage output in a high precision and a wide dynamic range. The circuit structure is shown in Figure 11, which realizes fast-changing high-voltage output from 0.5 V to 3800 V. With the range segmentation technology, we used 12 V as the bias power supply in the output voltage range of 0.5 V~12 V, which on the one hand solves the problem of the dark current of the optocoupler in the low voltage range, and on the other hand achieves a voltage control accuracy better than 10 mV. The high voltage range is 12 V~3800 V, with the main high voltage of 3850 V as the bias voltage, thus achieving a voltage control accuracy better than 1 V. The high-voltage optocoupler is for adjusting the output from a fixed high voltage to a variable high voltage. The high-voltage feedback circuit converts the output high voltage into a low voltage for closed-loop feedback control.

The digital acquisition, processing, and control unit controls the operation of the instrument according to the parameter table stored in EEPROM, collects and counts the output signal of the preamplifier, controls the required high voltage of the high-voltage circuit output through the DA converter, and controls the AD converter to collect analog engineering parameters, handles in-orbit preprocessing of scientific data and sends them to the payload controller through the interface circuit, and receives the data sent by the payload controller and inject, analyze and execute them. The digital acquisition, processing,

and control unit adopts Actel's 500 K-gate antifuse FPGA (AX500-1CQ208), which features resistance to irradiation and single event upset and outstanding spatial adaptability without the need for external configuration of PROM.

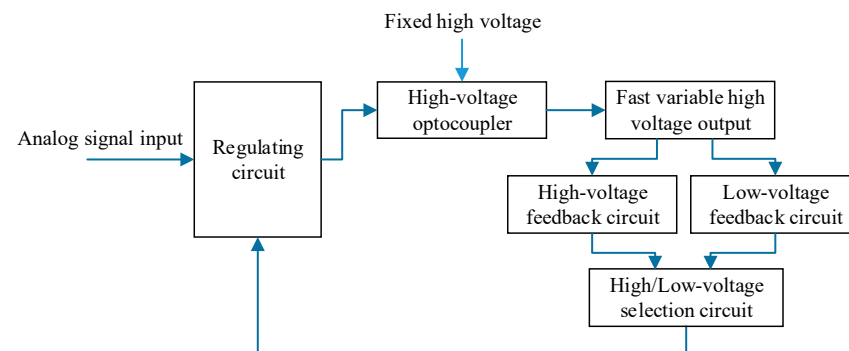


Figure 11. Structure of the fast variable high-voltage circuit in a large dynamic range.

4. Work Patterns and Data Products

In the in-orbit normal detection mode, there are 60 energy channels, 6 elevation angles, and a total of 360 slots in each working cycle (a slot is the minimum time unit for the detection of the instrument; during a slot, the high voltage is configured at a fixed value; and the configured high voltage of the instrument may differ from slot to slot). Each slot conducts counting and analysis for signals from 8-ion azimuthal angles and 8-electron azimuthal angles. The slot duration can be adjusted within the range of 2 ms to 400 ms based on the requirements. ESA high voltage varies for 60 steps in one working cycle (360 slots); DF1 and DF2 high voltages vary in each slot, and 6 slots are a working cycle. In each slot, the stabilization time of the electrostatic analyzer voltage and deflection voltage is less than 1 millisecond. When counting particles for statistical purposes, the instrument only tallies the particle counts during the voltage stabilization time within each slot. Since the electrostatic analyzer voltage and deflection voltage are sampled only once in each slot, the deflection voltage appears linear in Figure 12, while the actual voltage undergoes step changes. The high voltage in the in-orbit detection mode of the instrument is logarithmically spaced. We adopted rise and fall sweeping to prevent the sudden change of high voltage from the lowest to the highest. A complete cycle of high-voltage sweep is shown in Figure 12.

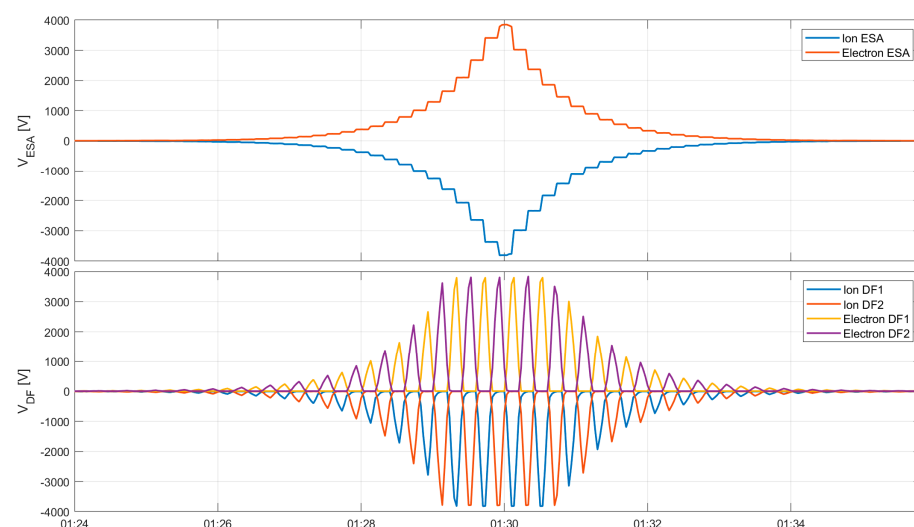


Figure 12. In-orbit data of electrostatic analyzer voltage sweep (Upper) and deflection voltage 1/2 rise and fall sweep (Lower).

5. Ground-Based Test and Calibration

The test of the plasma analyzer requires electron and ion sources with stable flux in a wide energy range to simulate space plasma [14]. Supported by the technological transformation of FY-4A, the National Space Science Center, CAS has established a complete set of internationally advanced vacuum testing systems for low-energy particles and surface charge and discharge, which are capable of providing electron, ion, and ultraviolet beams featuring different energies and components and controllable fluxes. The stable three-axis turntable inside the test system enables the instrument to be rotated freely, thus realizing the detectable range of energy and field of view for the detection of the absolute potential probe and then inverting the detectable range of absolute potential.

The basic performance parameters of the low-energy particle and surface charge-discharge vacuum test system are listed in Table 4, and the system is illustrated in Figure 13.

Table 4. Technical parameters of low-energy particle and surface charge-discharge vacuum test system.

Parameter	Scope
Electron beam energy	100 eV~30 keV
Ion beam energy	100 eV~30 keV
Beam source energy spread:	better than 10.0%@energ > 200 eV better than 20 eV@100 ev < energy < 200 eV
Beam spot diameter:	>70 mm
Ion components	H+, He+, N+, O+, Ar+, etc.
Beam source flux	$10^3 \sim 10^{10} \text{ cm}^{-2} \text{ s}^{-1}$
Vacuum	better than $5 \times 10^{-5} \text{ Pa}$
Vacuum turntable	the rotation covers $180^\circ \times \pm 45^\circ$, the translation repositioning accuracy is better than 0.1 mm, and the rotation repositioning accuracy is better than 0.1° .



Figure 13. Low-energy particle and surface charge-discharge vacuum test system.

The calibration of the FY-3 dawn–dusk orbit satellite plasma analyzer covers:

- (1) number of detection channels;
- (2) electrostatic analyzer factor and detectable energy range;
- (3) detectable field of view range at azimuth angles;
- (4) detectable field of view range at elevation angles;
- (5) sampling rate of the instrument;
- (6) ground-based calibration experiment accuracy.

For the calibration of the number of detection channels, we configured the internal memory state of the plasma analyzer to generate 96 sweep voltage steps of the electrostatic analyzer and compared the measured value with the set value to check the calibration accuracy. For the calibration of the energy range and the geometric factor of the ion analyzer, we used Ar⁺ ion sources calibrated at energy points of 3 keV, 5 keV, 10 keV, and 15 keV; for the calibration of the energy range and the geometric factor of the electron analyzer,

we used electron sources calibrated at energy points of 1 keV, 5 keV, 10 keV, and 15 keV; the energy accuracy is measured by the ground-based calibration equipment, and the energy ground-based calibration accuracy of ions and electrons is $\leq 3.53\%$ and $\leq 5.31\%$ respectively. For the calibration of the azimuth field of view, we adopted ion/electron beam sources of fixed energy, flux, and direction and recorded the response of the instrument in the azimuthal field of view; for the calibration of the elevation field of view, we realized different incident elevation angles through voltage sweep of the upper and lower deflection plates, and the repositioning accuracy of the turntable of the ground-based calibration equipment is 0.1° . The final results of the calibration experiment of the plasma analyzer are shown in Table 5 [15].

Table 5. Calibration experiment results of the plasma analyzer.

Item	Result
Energy range	Ion: 24.3 eV~32.4 keV Electron: 23.7 eV~31.6 keV
Energy resolution ($\Delta E/E_0$)	Ion: 0.180@10 keV Ar+ Electron: 0.171@10 keV Ele
Geometric factor	$3.48 \times 10^{-4} \text{ cm}^2\text{srev/ev}$
Observation channel	16×6
Detection accuracy	Azimuth: $\leq 0.44\%$ Ion energy: $\leq 3.53\%$ Ion elevation angle: $\leq 10.00\%$ Electron energy: $\leq 5.31\%$ 16×6

The calibration results show that the performance of the instrument meets the required indexes of the mission. Compared with the plasma analyzer (a comprehensive potential detector in the GEO orbit) of FY-4A, which was launched in 2016, it witnessed notable improvements in the detectable range of absolute potentials, sensitivity, detectable field of view, and angular resolution. The in-orbit observations show that the scientific detection data of the plasma analyzer are true and valid. The FY-3E satellite plasma analyzer is capable of real-time monitoring of the thermal plasma environment in the orbital space of the satellite and may provide supporting data for research on space weather forecasts and in-orbit safety assurance of the satellite.

6. Conclusions

The surface potential detector of the FY-3 dawn–dusk orbit satellite is a comprehensive instrument adopting the technology of reverting satellite absolute potential through plasma energy spectra and is applied to the LEO satellite for the first time in China. While measuring the absolute potential and differential potential of the satellite, it can also monitor the space plasma environment in low-Earth orbit, thus contributing to the safety of other satellites and spacecraft (astronauts) in the low-Earth orbit. The technical indicators measured in the laboratory verified the effectiveness of the instrument design and laid a foundation for the subsequent design of relevant payloads in China.

Author Contributions: Conceptualization, Z.T. and L.K.; methodology, A.Z.; software, X.Z.; validation, B.S. and Y.L.; formal analysis, B.L. and W.W.; investigation, J.G.; resources J.D. and C.L.; data curation, L.M.; writing—original draft preparation, L.M.; writing—review and editing, L.M.; visualization, B.L.; supervision, Z.T.; project administration, L.K.; funding acquisition, A.Z. All authors have read and agreed to the published version of the manuscript.

Funding: This research was funded by the Strategic Priority Research Program of the Chinese Academy of Sciences (Grant No. XDA17010303), the National Natural Science Foundation of China (NSFC, Grant No. 41204128), and the Foundation of the Key Laboratory of National Defense Science and Technology, Chinese Academy of Sciences (CXJJ-22S031).

Institutional Review Board Statement: Not applicable.

Informed Consent Statement: Not applicable.

Data Availability Statement: The data are not publicly available since the satellite was in the in-orbit test phase during the data period referenced in this article. The data presented in this study can be obtained upon request from the corresponding authors. The space weather Dst indices are available at <https://wdc.kugi.kyoto-u.ac.jp/> (accessed on 27 September 2023).

Acknowledgments: The research team extends its sincere gratitude to Xiaoxin Zhang, Cong Huang, Jiawei Li, and Dan Du from the China Meteorological Administration for their unwavering support in this research endeavor. Additionally, we would like to convey our heartfelt thanks to Jinhua Wang, Yong Yang, and Pengfei Zhang from the Shanghai Institute of Satellite Engineering for their invaluable assistance and guidance with the FY-3E Satellite Plasma Analyzer. In particular, we offer our sincere thanks to the reviewers for their valuable and helpful comments.

Conflicts of Interest: The authors declare no conflict of interest.

References

1. Eyre, J. *The WMO Vision for Global Observing Systems in 2025: To What Extent Will It Be Met by Space Agencies' Plans*; WMO: Geneva, Switzerland, 2015. Available online: <https://www.ecmwf.int/sites/default/files/elibrary/2015/9328-wmo-vision-global-observing-systems-2025-what-extent-will-it-be-met-space-agencies-plans.pdf> (accessed on 7 November 2023).
2. Yang, J.; Zhang, P.; Lu, N.; Yang, Z.; Shi, J.; Dong, C. Improvements on global meteorological observations from the current Fengyun 3 satellites and beyond. *Int. J. Digit. Earth* **2012**, *5*, 251–265. [CrossRef]
3. Cao, J.B.; Wang, X.Y.; Zhou, G.C.; Chen, T. Plasma sheath of moving spacecraft in magnetized plasma of low earth orbit. *Chin. Journal Geophys.* **2000**, *43*, 491–495. [CrossRef]
4. Greenspan, M.E.; Anderson, P.B.; Pelagatti, M. *Characteristics of the Thermal Plasma Monitor (SSIES) for the Defense Meteorological Satellite Program (DMSP) Spacecraft S8 through S10*; Report AFGL-TR-86-0227; Air Force Geophysics Lab, Hanscom Air Force Base: Bedford, MA, USA, 1986.
5. McFadden, J.P.; Carlson, C.W.; Larson, D.; Ludlam, M.; Abiad, R.; Elliott, B.; Turin, P.; Marckwordt, M.; Angelopoulos, V. The THEMIS ESA Plasma Instrument and In-flight Calibration. *Space Sci. Rev.* **2008**, *141*, 277–302. [CrossRef]
6. Evans, D.S.; Greer, M.S. *Polar Orbiting Environmental Satellite Space Experiment Monitor-2: Instrument Description and Archive Data Documentation*, NOAA Technical Memorandum, Version 1.3; NOAA Environmental Center: Boulder, CO, USA, 2004.
7. Anderson, P.C. Characteristics of spacecraft charging in low Earth orbit. *Geophys. Res.* **2012**, *117*, A07308. [CrossRef]
8. Pollock, C.; Moore, T.; Jacques, A.; Burch, J.; Gliese, U.; Saito, Y.; Omoto, T.; Avannov, L.; Barrie, A.; Coffey, V.; et al. Fast plasma investigation for magnetospheric Multiscale. *Space Sci. Rev.* **2016**, *199*, 331–406. [CrossRef]
9. McComas, D.J.; Alexander, N.; Allegrini, F.; Bagenal, F.; Beebe, C.; Clark, G.; Cravay, F.; Desai, M.I.; De Los Santos, A.; Demkee, D.; et al. The ovian Auroral Distributions Experiment (ADE) on the uno Mission to upiter. *Space Sci. Rev.* **2017**, *213*, 547–643. [CrossRef]
10. Carlson, C.W.; Curtis, D.W.; Paschmann, G.; Michel, W. An instrument for rapidly measuring plasma distribution functions with high resolution. *Adv. Space Res.* **1983**, *2*, 67–70. [CrossRef]
11. Young, D.T.; Bame, S.J.; Thomsen, M.F.; Martin, R.H.; Burch, J.L.; Marshall, J.A.; Reinhard, B. 2-Pi-radian field-of-view toroidal electrostatic analyzer. *Rev. Sci. Instrum.* **1988**, *59*, 743–751. [CrossRef]
12. Moldosanov, K.A.; Kashirin, V.A.; Skrynnikov, A.M.; Anisimova, I.A.; Anisimov, V.P.; Kobtsov, G.A. Black coatings for stray light and thermal control applications. *Proc. SPIE—Int. Soc. Opt. Eng.* **2001**, *4458*, 87–94. [CrossRef]
13. Goueffon, Y.; Arurault, L.; Mabru, C.; Tonon, C.; Guigue, P. Black anodic coatings for space applications: Study of the process parameters, characteristics and mechanical properties. *J. Mater. Process. Technol.* **2009**, *209*, 5145–5151. [CrossRef]
14. Kong, L.; Zhang, A.; Tian, Z.; Zheng, X.; Wang, W.; Liu, B.; Wurzel, P.; Piazza, D.; Etter, A.; Su, B.; et al. Mars Ion and Neutral Particle Analyzer(MINPA) for Chinese Mars Exploration Mission(Tianwen-1): Design and ground calibration. *Earth Planet. Phys.* **2020**, *4*, 333–344. [CrossRef]
15. Wang, X.; Zhang, X.; Wang, J.; Huang, C.; Li, J.; Zhang, A.; Kong, L.; Du, D.; Yang, Y.; Zhang, P.; et al. Plasma Analyzer for the Chinese FY-3E Satellite: In-Orbit Performance and Ground Calibration. *Atmosphere* **2023**, *14*, 1665. [CrossRef]

Disclaimer/Publisher's Note: The statements, opinions and data contained in all publications are solely those of the individual author(s) and contributor(s) and not of MDPI and/or the editor(s). MDPI and/or the editor(s) disclaim responsibility for any injury to people or property resulting from any ideas, methods, instructions or products referred to in the content.